Article

Photodegradation of 1-Butyl-3-methylimidazolium Chloride [Bmim]Cl via Synergistic Effect of Adsorption–Photodegradation of Fe-TiO₂/AC

Azhar Zawawi [iD]**, Raihan Mahirah Ramli * ** [iD] **and Noorfidza Yub Harun**

Department of Chemical Engineering, Universiti Teknologi PETRONAS, 32610 Bandar Seri Iskandar, Perak, Malaysia; azharz.utp@gmail.com (A.Z.); noorfidza.yub@utp.edu.my (N.Y.H.)
* Correspondence: raihan.ramli@utp.edu.my; Tel.: +60-53-687-553

Abstract: Ionic liquids (ILs) have attracted interest among researchers due to their tunable properties, which enable them to be used in a wide variety of applications. However, toxicity and biodegradation studies of ILs proved that most of the aromatic ILs, such as imidazolium, are highly toxic and non-biodegradable. Researchers have investigated several advance oxidation processes (AOPs) in order to evaluate the efficiency of the systems used to remove ILs from wastewater. However, their relatively high cost and environmental concerns have limited the application of these AOPs in industry. This research conducted a photocatalytic study using hybrid nanomaterials to evaluate the efficiency of this system as an alternative AOP system for the removal of ILs from wastewater. The synergistic effect of adsorption–photodegradation was introduced by depositing Fe-TiO₂ onto functionalized activated carbon (AC). Nano-TiO₂ was synthesized using the microemulsion method, then modified with a transition metal, and deposited onto oxidized AC. The photodegradation reaction of 1-butyl-3-methylimidazolium chloride [bmim]Cl was then investigated under simulated visible light irradiation. It was observed that the overall efficiency of the system increased with the increasing amount of Fe loading. Our investigation revealed that extrinsic factors such as solution pH, the initial concentration of ILs, and photocatalyst dosage significantly affect the overall efficiency of the system. The optimum condition for the system was observed at pH 10, with initial ILs at 1 mM at 1 g/L of photocatalyst. The best performance photocatalyst was 0.2Fe-TiO₂/AC.

Keywords: photodegradation; TiO₂; ionic liquids; activated carbon; synergistic effect

1. Introduction

Ionic liquids (ILs) are chemicals that can be synthesized via the metathetic exchange of anion, neutralization with Brønsted acid, direct alkylation and alkylimidazole, or a carbonate route [1]. Depending on its specific applications, the physical and chemical properties of ILs are tunable by varying its cation and anion. ILs are currently being used in industry for both large-scale production and pilot plant studies. For instance, Petroliam Nasional Berhad (PETRONAS) has applied ILs for mercury removal processes, while BASF and the Institutes Francis de Petrole Axens (IFP) have employed ILs in biphasic acid scavenging ionic liquids (BASIL) process and dimersol process, respectively [2].

The increasing number of IL applications has raised concerns regarding the impact of ILs on the environmental due to its high solubility and resistivity in water. A few researchers who conducted biodegradation studies on ILs concluded that ILs with an aromatic ring cation, such as imidazolium, are non-biodegradable [3–5]. Yet, this type of IL has been widely used in bio-industry [1]. Hence, an efficient treatment system that is able to overcome the high solubility properties of ILs in water is urgently required. Advance oxidation processes (AOPs) are widely known for its high efficiency to

degrade wide range of organic pollutants [6]. Photocatalytic degradation employing a semiconductor as the photocatalyst is one of the AOPs that efficiently degrades ILs in wastewater [7]. This process can be considered relatively low cost and sustainable, since it is able to convert renewable solar energy into a chemical reaction [8].

Among the semiconductors available for this application, titania (TiO_2) is the most researched semiconductor that is used as a photocatalyst [9]. However, the major drawback of TiO_2 that hinders its application in industry as a photocatalyst is its limited range of UV light absorption. In addition, TiO_2 has a comparatively slow diffusion rate between the target pollutant and its surface [10,11]. These limitations could be overcome through the modification of TiO_2 via several methods, such as modification with metals, depositing TiO_2 onto activated carbon (AC) as a support or coupling another semiconductor onto TiO_2 as a co-catalyst [12,13]. The introduction of metal loadings onto TiO_2 has significantly enhanced its activity under visible light, thus improving the overall performance of the system [9]. The modification process causes defects to the TiO_2 structure such as oxygen vacancy (V_o) and Ti^{3+}, which lead to the reduction of band gap energy. Hence, the absorbance of TiO_2 is shifted towards the visible light region [14].

Furthermore, the addition of activated carbon to TiO_2 has a dual function: as a support, and at the same time, as the center of accumulation for the pollutant. The presence of hydroxyl groups (–OH) on the AC surface is able to attract 1-butyl-3-methylimidazolium chloride ([bmim]Cl) towards the surface of the photocatalyst, and thus enhances the diffusion rate of [bmim]Cl into TiO_2. The synergistic effect of the adsorption–photodegradation of the composite photocatalyst consequently increases the overall efficiency of the system [15]. Apart from intrinsic factors, the extrinsic factors such as the initial ILs concentration, the initial pH of the ILs solution, and photocatalyst dosage have been reported to have significant effects on the overall efficiency of the systems [16].

In this paper, the work is focused on the development of hybrid nano-photocatalysts that consist of nano-TiO_2 synthesized via the microemulsion method, modified with Fe, and deposited onto the AC surface. The efficiency of the developed photocatalyst was evaluated in a photocatalytic degradation system containing [bmim]Cl solution at the desired concentration under a 500-W visible light energy source. Several parameters that were reported to be highly significant to the photodegradation process will be investigated.

2. Materials and Methods

2.1. Materials

All of the chemicals were purchased and used without further purification. Hexanol ($C_6H_{14}O$, 98%), iron (III) nitrate nonahydrate ($Fe(NO_3)_3 \cdot 9H_2O$), 1-butyl-3-methylimidazolium chloride, [bmim]Cl ($C_8H_{15}ClN_2$), heptane (C_7H_{16}, 99%), Ethanol (C_2H_3OH, 95%) and titanium tetraisopropoxide (TTIP, $C_{12}H_{28}O_4Ti$, 97%) were purchased from Merck (Darmstadt, Germany). Meanwhile, other chemicals such as nitric acid (HNO_3, 65%), triton X-100 ($C_{34}H_{62}O_{11}$, AR), potassium dihydrogen phosphate (KH_2PO_4), phosphoric acid (H_3PO_4, 85%) and triethylamine ($C_6H_{15}N$, AR) were supplied by R&M Chemicals (Semenyih, Malaysia)

2.2. Methods

Nano-TiO_2 was synthesized using the water-in-oil microemulsion method, as reported in a previous study [7], followed by modification with the desired Fe via the wetness impregnation method. The resultant powder from the impregnation method was calcined at 400 °C for 1.5 h. In a different set-up, the pre-carbonized AC was oxidized using 1 M of nitric acid in a boiling condition for 20 min. The oxidized AC was washed repeatedly with distilled water until the filtrate became neutral. The oxidized AC was then dried overnight in an oven at 80 °C. Finally, the developed Fe-TiO_2 and AC were mixed (10 wt % AC) using the impregnation method, as reported in our previous study [17].

The final photocatalyst was denoted as *a*Fe, where *a* refers to the amount of Fe i.e., 0.2Fe refers to 0.2 wt % Fe deposited onto TiO_2/AC.

2.3. Characterization of the Photocatalyst

Characterization of the photocatalyst was conducted to analyze its physical and chemical properties. The effect of adding AC to the photocatalyst surface was evaluated by analyzing the existing functional group using Fourier transform infrared (FTIR) spectroscopy. The analysis was conducted using a Shimadzu FTIR-8400S Spectrophotometer (Kyoto, Japan). The absorbance and band gap of the photocatalyst was conducted using UV-Visible Spectroscopy. An optical property of the photocatalyst was conducted using an Agilent Technologies Cary 100 UV-Vis Spectrophotometer Model G9821A (Santa Clara, CA, USA). The pH_{PZC} of the photocatalyst was employed using the mass titration method, as reported in a previous study [18]. Crystallinity and average particle size analysis of the photocatalyst were conducted using Bruker D8 Advanced XRD (Billerica, MA, USA) with Cu Kα radiation (40 kV, 40 mA) at 2θ angles from $10°$ to $80°$.

2.4. Photodegradation Study

The performance of the developed photocatalyst was evaluated in the photocatalytic degradation of [bmim]Cl using an open glass reactor in ambient conditions. In a typical experiment, a pre-determined amount of photocatalyst was added into the reactor containing the desired concentration of [bmim]Cl solution. The system was stirred in dark for 30 min to allow for an equilibrium adsorption–desorption process, followed by 2 h irradiation under a 500-W halogen lamp. Liquid samples were collected at regular time intervals and analyzed using high performance liquid chromatography (Agilent 1100 HPLC, Santa Clara, CA, USA). For better separation and sharp analysis, column symmetry C-18 (250×4.6 mm, 5 μm) and a mobile phase mixture of methanol (35 vol %) and 25 mM of phosphate buffer (KH_2PO_4/H_3PO_4) containing 0.5% of triethylamine were used. The analysis was performed at a column temperature of 30 °C, a 5-μL sample injection, and an 0.8 mL/min flow rate. The separated [bmim]Cl was detected at a 212-nm wavelength using a UV detector (Agilent, Santa Clara, CA, USA)

3. Results and Discussion

3.1. Characterization of the Photocatalysts

3.1.1. Fourier Transform Infrared (FTIR)

Figure 1 shows the vibration peak of different photocatalysts with respect to the Fe content. From the figure, the first broader peak recorded at 766 cm^{-1} could be ascribed to the titania framework that had been deposited onto the AC, such as Ti–O–Ti [15,19,20]. However, the intensity of the vibration IR spectra decreased as the amount of Fe increased. Several studies have reported observations where the IR spectrum of ferric oxide (Fe_2O_3) between 560–460 cm^{-1} may have overlapped with the Ti–O–Ti vibration peak at 766 cm^{-1}, causing this peak to diminish as the amount of Fe increased [21,22]. The vibration peak recorded at 1390 cm^{-1} represented the C=O stretching related to carboxylic groups and carboxylate moieties [23,24], while the presence of C=O stretching could be due to the oxidation treatment of AC with nitric acid. This peak was not recorded for lower concentrations of Fe. The same finding was also recorded by Liu et al. in their study where a higher intensity of vibration carbonaceous peaks was recorded only for higher percentages of metal loading [25]. The study also stated that the usage of acid as a treatment agent could produce the homogenous distribution of titania with a complex structure [23]. This can be supported with a vibration peak around 766 cm^{-1}, which shows a strong vibration of Ti–O, especially for lower amounts of Fe, and proves that complex TiO_2 is well distributed on the surface of AC [26].

The small and sharp vibration peaks of C–H have been detected in IR spectra at wavenumber 1390 cm^{-1} and 1478 cm^{-1}. These peaks show that the dissociation of precursor TiO_2/AC may occur,

leaving behind other species such as O, Ti, and C. The presence of the C–H bond is also stated to be chemisorbed [27]. Similarly to the C=O vibration, the C–H peak was not detected for lower amounts of Fe. Meanwhile, the peak at 1640 cm^{-1} represents the vibration of O–H that may have come from the adsorption of H$_2$O onto the surface of the photocatalyst [15,26,27]. A small peak detected at 2412 cm^{-1} represents the double bond that may be present on the surface of photocatalysts such as C=O [27]. Two close vibration peaks at 2956 cm^{-1} and 2974 cm^{-1} also represent the O–H stretching that may be present from the oxidation of AC. This vibration does not appear in IR spectra for low amounts of Fe. The broader peak at 3454 cm^{-1} represents the O–H group [15,26,27]. The presence of this broader peak shows the high vibration of O–H that exists on the AC's surface, which has been oxidized with nitric acid. This is in line with the purpose of oxidation treatment, which is to obtain a more hydrophilic surface for the photocatalyst with an oxygen-containing functionalized group on the surface of AC, such as the O–H group [23]. In the adsorption study of hydrophobic ILs, the presence of O–H is important, as it could act as a pollutant concentrator for the composite photocatalyst. The O–H groups that were present on the surface of the photocatalyst were able to promote the H-bonding interactions with the anions of hydrophobic ILs [28,29].
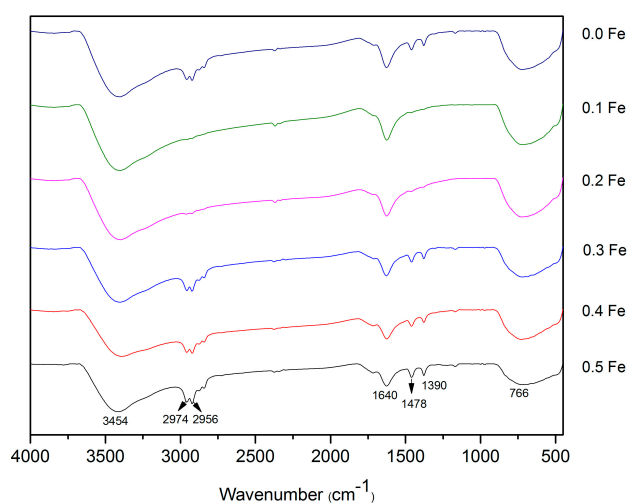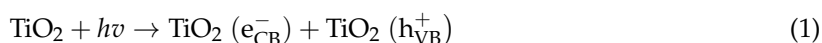

Figure 1. Fourier transform infrared (FTIR) spectra of the photocatalyst at different amounts of Fe.

3.1.2. Diffuse Reflectance UV-Visible (DRUV-Vis) Analysis

The absorption spectra of the photocatalysts at different amounts of Fe are presented in Figure 2. From the figure, the absorption edge of TiO$_2$ is at approximately 400 nm, which is correlated to a band-gap energy (E$_g$) of 3.10 eV. Meanwhile, for the photocatalyst named 0.0Fe (which is the composite of TiO$_2$ and AC), the absorption edge was significantly green-shifted to a 500-nm wavelength corresponding to ca. 2.48 eV. The presence of 10 wt % AC in the composite has a major role in the reduction of E$_g$, where the powdered photocatalyst was greyish compared to bare TiO$_2$, which is white. On the other hand, the addition of 0.1 wt % Fe onto the TiO$_2$/AC slightly blue-shifted the absorption edge, which corresponded to an E$_g$ value of 2.88 eV. A further shift of the absorption edges could be observed as the amount of Fe loadings increased, with the lowest E$_g$ recorded for the photocatalyst with 0.5 wt % Fe. The summary of E$_g$ is presented in Table 1.

This observed shift could be ascribed to the excitement of electron (e$_{CB}^-$) from the valence band (VB) of TiO$_2$, as described by Equations (1) and (2) [30]. The h$_{VB}^+$ and trapped electron (*et*) refer to the hole formed at VB after the excitement of e$_{CB}^-$, and the electron that had been trapped on the surface AC and metal loading, respectively.

$$TiO_2 + hv \rightarrow TiO_2 \ (e_{CB}^-) + TiO_2 \ (h_{VB}^+) \tag{1}$$

$$TiO_2 \left(e_{CB}^-\right) \rightarrow TiO_2 \left(et\right) \tag{2}$$

The trapped electron could also occur from e_{CB}^- to Fe on the photocatalyst before the *et* is excited again to the TiO_2 surface, and as a result increase the absorbance value of the UV-Vis (3–6). The e^- refers to the electron from Fe itself.
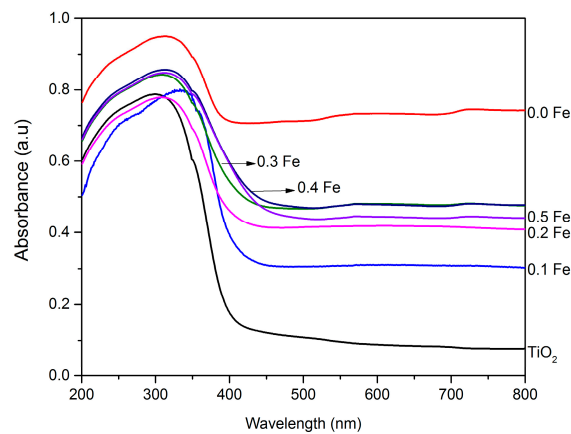
$$Fe^{3+} + TiO_2 \left(e_{CB}^-\right) \rightarrow Fe^{2+} \tag{3}$$

$$Fe^{2+} \rightarrow Fe^{3+} + TiO_2(et) \tag{4}$$

$$Fe^{3+} \rightarrow Fe^{4+} + e^- \tag{5}$$

$$Fe^{4+} + TiO_2(et) \rightarrow Fe^{3+} \tag{6}$$

Figure 2. Diffuse reflectance spectra of the photocatalyst.

Table 1. Band-gap energy (E_g) of the photocatalyst.

Photocatalyst	Band-Gap Energy, E_g (eV)
TiO_2	3.10
0.0Fe	2.48
0.1Fe	2.88
0.2Fe	2.64
0.3Fe	2.61
0.4Fe	2.39
0.5Fe	2.36

3.1.3. X-ray Diffraction (XRD)

Figure 3 depicts the XRD chromatogram for the bare TiO_2, AC, and also the composite photocatalyst.

From Figure 3, a similar pattern of XRD pictograph was recorded for the composite photocatalyst in comparison with bare TiO_2. From the figure, it can be clearly observed that both bare and composite TiO_2 consist of an anatase structure (98-015-4610) with peaks at 25.3°(101), 37.8°(111), 48.0°(200), 55.1°(121), 62.7°(215), 70.3°(220), 75.1°(125) and 82.7°(224). The amorphous carbon structure reveals two distinct peaks at 24.6°(002) and 43.9°(110), which proves the successful production of AC via the described method in Section 2.2. However, these degrees diminish after depositing TiO_2 onto AC, could be due to the dominant peak of anatase TiO_2 [31]. In addition, no peak related to Fe_2O_3 was detected, even at the highest amount of Fe loading (0.5 wt %), which shows that Fe was uniformly distributed on the TiO_2 surface. Furthermore, Fe and Ti possess similar ionic radii (Ti = 0.68 Å and Fe = 0.64 Å) [32,33]. The mean particle size of the composite photocatalysts was calculated using the

Scherrer equation [34] at the dominant peak of anatase ($2\theta = 25.3$). Table 2 summarizes the physical properties of the photocatalyst from XRD analysis.
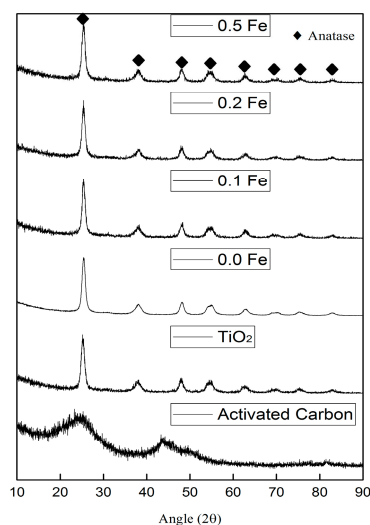
Figure 3. XRD analysis for the photocatalyst with different amounts of Fe content.

Table 2. Particle size of the composite photocatalyst.

Photocatalyst	Particle Size (nm)	Crystallographic Constant (Å)
TiO_2	8.30	a = 3.8000, b = 3.8000, c = 9.4600
AC	29.30	a = 2.4700, b = 2.4700, c = 6.9300
0.0Fe	24.20	a = 3.8000, b = 3.8000, c = 9.5020
0.1Fe	10.30	a = 3.7850, b = 3.7850, c = 9.5010
0.2Fe	10.70	a = 3.7850, b = 3.7850, c = 9.4440
0.5Fe	11.20	a = 3.7850, b = 3.7850, c = 9.4820

It is noteworthy to mention that bare TiO_2 has the smallest crystallite size, while AC has triple the value. When TiO_2 was deposited onto AC (0.0Fe), the crystallite size of the photocatalyst was 24.2 nm, similar to the sizes for AC. Adding 0.1 wt % Fe significantly reduced the crystallite growth by 57%, causing smaller crystals than 0.0Fe. Similar findings were reported by Li et al., where the particle size of tungsten W–TiO_2 loaded onto AC was found to be lower than the crystallite size of TiO_2/AC only. This is because Fe^{3+} could penetrate into the Ti^{4+} lattice causing distortion in the structure; thus, it favored the smaller particle size of the photocatalyst, as confirmed by the crystallographic data in Table 2 [35]. The c value for the composite reduced compared to bare TiO, which proved that changes occurred in the crystallographic structure of the composite photocatalysts. A reduction in particle size could govern the photodegradation process, as proven in a previous study [36]. On the other hand, the increasing amount of Fe from 0.1 wt % to 0.5 wt % has slightly increased the crystallite size of the photocatalyst, which contradicts with the reported observations from previous studies [35]. The increasing size of the crystals could be due to the agglomeration of Fe_2O_3 and TiO_2 during the calcination process, yet the amount of Fe is very low, and highly dispersed on TiO_2 for it to be detected by XRD analysis [37].
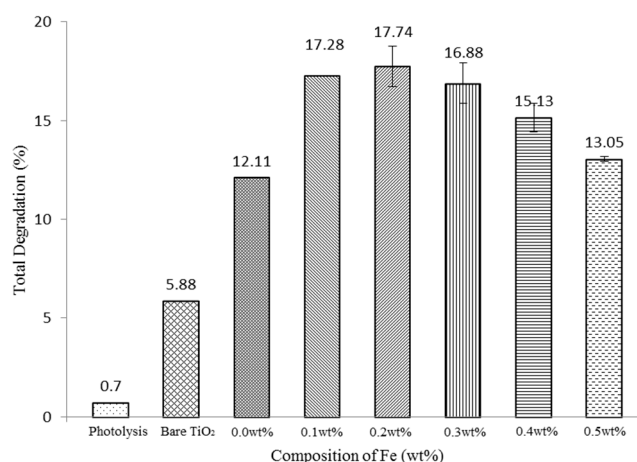
3.2. Photodegradation Study

The photocatalytic activity of the synthesized photocatalyst was evaluated in the photodegradation system of [bmim]Cl under visible light radiation. A 500-W halogen lamp was used to simulate solar light, with the main light spectrum between 400–600 nm. The effect of each

parameter i.e., the composition of Fe, initial concentration of [bmim]Cl ([IL_o]), initial pH of the solution, and photocatalyst dosage ([photocatalyst]) were evaluated using one-factor-at-a-time (OFAT) method.

3.2.1. Effect of Fe Composition

The effect of varying Fe amounts on the total degradation efficiency of the system is summarized in Figure 4. Insignificant degradation was observed when no photocatalyst was added into the system, while only 5% degradation was recorded in the system containing bare TiO_2. Significant enhancement was observed when Fe was added to the photocatalyst. The addition of Fe is crucial to form a space charge layer on the TiO_2 surface where upon light radiation, the generated electron (e_{CB}^-) will be trapped by the Fe, thus preventing it from recombining with the hole (h_{VB}^+). Based on the classical field theory, the formation of Fe^{2+} and Fe^{4+} is very unstable. This is because in their molecular state 3d5 configuration, they are only occupied with half-filled electrons. Hence, the charge carrier then migrated to the surface of TiO_2 to degrade [bmim]Cl. The Fe^{2+} can be returned back to Fe^{3+} by donating one (e_{CB}^-) either directly to [bmim]Cl or to H_2O to undergo a reduction process, producing strong free radicals such as the hydroxyl radical ($^\bullet OH$). These radicals are active species that are able to attack a wide range of organic pollutants, and thus further enhance the degradation rate of pollutants. Meanwhile, Fe^{4+} can be transformed to Fe^{3+} by receiving an electron or losing a hole (h_{VB}^+). The h_{VB}^+ will come into contact with the oxygen (O_2) that has also been adsorbed on the surface of TiO_2, leading to the formation of the superoxide radical ($O_2^{-\bullet}$) [14,38]. During the degradation process of [bmim]Cl, the $O_2^{-\bullet}$ will attack C2, C4, and C5 of the imidazolium ring to produce an unstable by-product known as 1-alkyl-3-methyl-2,4,5-trioxoimidazolidine. The formation of these by-products means that the first stage of the degradation process where the phenomenon opening ring of cation occurred [39].

Figure 4. Efficiency of [bmim]Cl photodegradation system with different compositions of Fe; [IL_o] = 5 mM, pH = 8 and [photocatalyst] = 1 g/L.

Further increasing the amount of Fe from 0.1 wt % to 0.2 wt % increased the surface barrier and lead to the optimum separation of the $e_{CB}^- - h_{VB}^+$ pairs. However, when the amount of Fe was increased beyond its optimum amount, the overall efficiency of the system decreased. Even though the higher amount of Fe further reduced the band-gap energy of TiO_2 (Table 1), it also acted as the recombination center for the charge carriers. The excess amount of Fe reversed its positive role and become the recombination sites for the $e_{CB}^- - h_{VB}^+$ pairs, thus preventing them from taking part in the degradation process [40]. Similar findings have been discussed by other researchers, where higher Fe contents could produce more Fe clusters on the TiO_2 surface, as seen in Equations (3)–(6) [41]. The formation of Fe_2O_3 could correlate with IR spectra (Figure 1), as the Ti–O–Ti vibration was slightly diminish at higher amounts of Fe due to overlapping with the Fe_2O_3 that was recorded from 464 cm^{-1} to 700 cm^{-1}. The formation of an oxygenated group on the surface of the composite photocatalyst

(Figure 1) also played an important role in the degradation of [bmim]Cl. The presence of functionalized groups such as O–H is believed to be able to increase the interaction of H-bonding between the surface of the composite photocatalyst and the anion Cl [29]. Hence, more [bmim]Cl will be attracted to the AC on the TiO_2 surface, which then enhances the diffusion rate between [bmim]Cl and the surface TiO_2, resulting in a significant increase in the total removal of [bmim]Cl. At the same time, the diminished carbonaceous peak for lower Fe loadings (1390 cm^{-1}) also may enhance the activity of the photocatalyst, as presence of this peak could reduce the catalytic property of the photocatalyst [42]. This clearly can be seen from Figure 4, where both 0.1Fe and 0.2Fe show slightly a higher removal of bmim[Cl] compared with the other photocatalyst, as the carbonaceous peak does not present for both photocatalysts.

3.2.2. Effect of Extrinsic Factor: Initial Concentration of [bmim]Cl (IL_o)

Figure 5 presents the effect of the initial concentration of [bmim]Cl ($[IL_o]$) on the overall performance of the system. The study was conducted by keeping other parameters constant i.e., 0.2 wt % Fe, with initial pH at 8 and 1 g/L of photocatalyst. In general, the overall degradation efficiency decreased with the increase of $[IL_o]$. At lower concentrations, a sufficient active site on the photocatalyst for optimal adsorption and degradation processes lead to the higher overall efficiency of the system. However, as the concentration of [bmim]Cl increased, the number of [bmim]Cl molecules in the solution consequently increased, causing lower absorption of photons and lower degradation rate on the surface of the photocatalyst due to insufficient active sites. On the other hand, at lower $[IL_o]$, the accumulation of the pollutant on the surface of TiO_2 reduced, providing a more active surface area to absorb the photons and generate the charge carrier. As more charge carriers are generated, more [bmim]Cl can be degraded. This phenomenon follows the Lambert law, whereas the concentration of organic molecules reduced, the path length taken by the photon to enter the solutions increased [43].
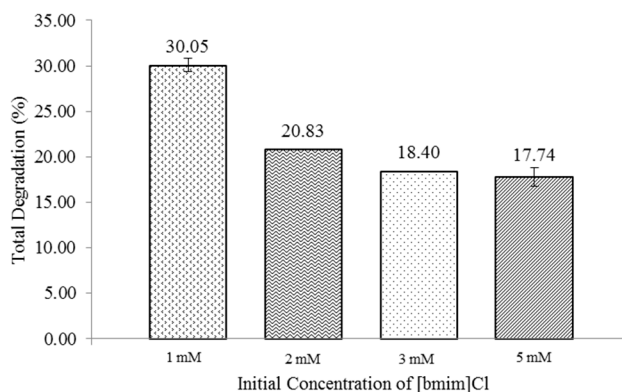

Figure 5. Efficiency of [bmim]Cl photodegradation system at different $[IL_o]$.

3.2.3. Effect of Extrinsic Factor: Initial pH of the [bmim]Cl Solution

The point zero charge (pH_{pzc}) of the photocatalyst can be defined as the limiting pH when the net surface charge of the photocatalyst is zero. The pH_{pzc} value of the photocatalyst was determined using the titration method as reported in a previous study [18].

Pursuant to Section 3.2.2, optimum $[IL_o]$ was observed at 1 mM. Hence, this $[IL_o]$ has been selected to study the effect of the initial pH of the [bmim]Cl solution, while keeping other parameters constant i.e., 0.2 wt % Fe, $[IL_o]$ at 1 mM, and 1 g/L of photocatalyst. Figure 6 depicts the comparative study on the pH of the [bmim]Cl solution. As the initial solution's pH increased, the total removal of [bmim]Cl increased until the optimum point, and then decreased. The lowest [bmim]Cl degradation was recorded in an acidic region at pH 3. In an acidic region, the surface charges of the photocatalyst and organic molecule were both protonated. The similar charges between both species made them

repel each other, causing less adsorbate to be adsorbed onto the surface of the photocatalyst. Further, this also caused a lower amount of [bmim]Cl to be degraded by the charge carrier [44]. In addition, the photocatalyst was reported to be agglomerated in acidic conditions, thus reducing the availability of the TiO_2 active site that can be used to absorb photons and adsorb [bmim]Cl [45]. From the study, the best working pH for the photodegradation of [bmim]Cl was recorded in alkaline condition at pH 10. In this condition, the OH^- interacted with h_{VB}^+, leading to the higher production of $\bullet OH$, and thus increased the degradation rate of [bmim]Cl. However, at even higher alkalinity, both the organic molecules and the surface of the photocatalyst were deprotonated. The similar charges of both species again repelled each other, causing less [bmim]Cl to be adsorbed on the surface of TiO_2, and hence reducing the total degradation [44]. This ionization of the surface charge photocatalyst in various pH conditions could be explained as in Equations (7) and (8) [9].

It can be observed that the pHpzc of the photocatalyst is 6.3 (Figure 7). On the other hand, the pH of the [bmim]Cl solution was recorded around 8.2 ± 0.2, regardless of the [bmim]Cl concentration. Generally, when the pH of the solution is higher than the pH_{pzc} of the photocatalyst, the surface of the photocatalyst will be negatively charged. Different charges between the photocatalyst surface and [bmim]Cl will attract each other, hence increase the diffusion rate of [bmim]Cl into TiO_2 [9]. On the other hand, similar charges between both entities will reduce the ability of TiO_2 to attract the [bmim]Cl compound toward its surface.
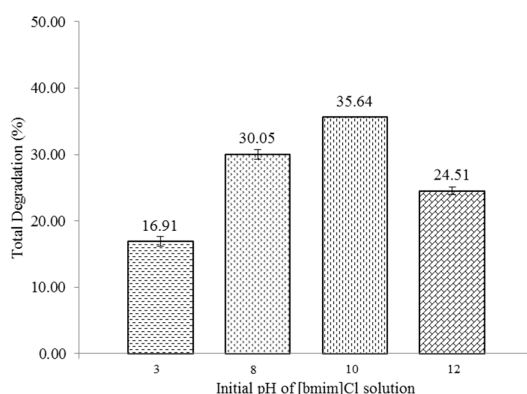
$$TiOH + H^+ \rightarrow TiOH_2{}^+ \qquad (7)$$

$$TiOH + OH^- \rightarrow TiO^- + H_2O \qquad (8)$$

Figure 6. Efficiency of [bmim]Cl photodegradation system at different initial pH of [bmim]Cl solution.
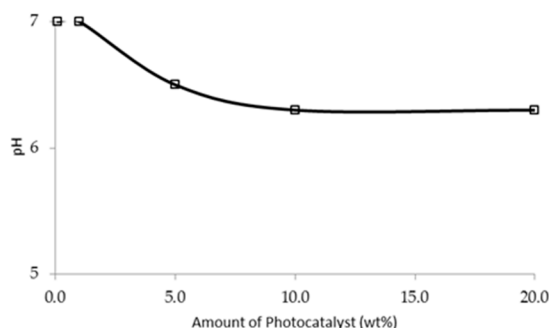

Figure 7. Surface charge of the photocatalyst $0.2Fe\text{-}TiO_2/AC$.

3.2.4. Effect of Extrinsic Factor: Dosage of Photocatalyst [Photocatalyst]

The effect of the photocatalyst dosage [photocatalyst] on the efficiency of the system was evaluated by keeping other factors constant i.e., 0.2 wt % Fe, $[IL_o]$ at 1 mM, and initial pH 10. Figure 8 summarizes

the removal efficiency at different [photocatalyst]; as can be observed from the figure, [photocatalyst] has a significant effect on the total removal of [bmim]Cl. The effect of the photocatalyst dosage [photocatalyst] on the overall efficiency of the photodegradation system of [bmim]Cl was studied by varying the [photocatalyst] between 0.0–8 g/L. From Figure 8, the total degradation of [bmim]Cl increased until the optimum [photocatalyst] was achieved. Insufficient amount of photocatalyst supplied to the system will cause a blockage of the active site by [bmim]Cl, causing poor efficiency of the system [46]. As the dosage increased, the active sites available for the photodegradation process also increased, leading to a higher degradation rate. Beyond the optimum dosage (>1 g/L), the overall efficiency of the system decreased despite a larger amount of photocatalyst being used in the system. A high amount of photocatalyst in the system lead to the screening phenomenon of particles, which will cause blockages of the active sites of the photocatalyst. Furthermore, excess amount of photocatalyst leads to agglomeration of the nanoparticles, thus reduces total surface area of the photocatalyst which then lead to lesser photon absorption [47].
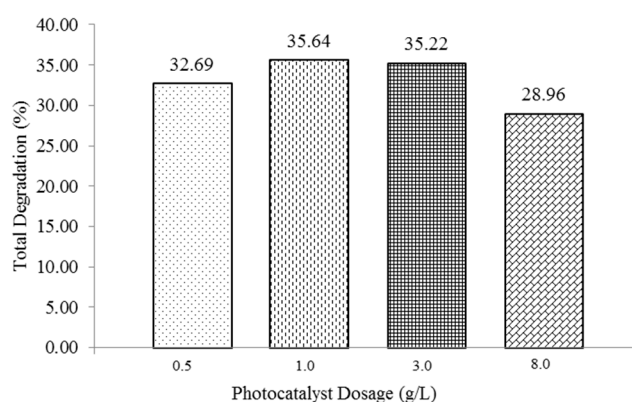
Figure 8. Efficiency of [bmim]Cl degradation system at different [photocatalyst].

4. Conclusions

Optimum amount of Fe in the preparation of photocatalyst is crucial as it could directly affect the efficiency of the system. From the analysis study of composition Fe loaded onto TiO_2, it can be concluded that incorporating an optimum amount of metal onto the surface of TiO_2 can shift the performance of TiO_2 into the visible region, and increase the performance of the photocatalyst for the removal of [bmim]Cl. Apart from Fe, concentration of the compound of interest, in this case, [bmim]Cl also is important. Excess $[IL_O]$ in the system will block the surface of TiO_2 from harvesting the light, thus causing lower overall efficiency. Optimum pH for the system to work at the highest efficiency was recorded at pH 10. At this condition, the available ^-OH will increase the production of $^\bullet OH$ as the attacking agent that will increase the total degradation of [bmim]Cl. Finally, optimum amount of photocatalyst itself is also critical as excess photocatalyst dosage will cause agglomeration leading to lesser active sites of the photocatalyst for further process.

Author Contributions: Azhar Zawawi and Raihan Mahirah Ramli conceived and designed the experiments; Azhar Zawawi performed the experiments; Azhar Zawawi and Raihan Mahirah Ramli and Noorfidza Yub Harun analyzed the data; Raihan Mahirah Ramli and Noorfidza Yub Harun contributed reagents/materials/analysis tools; Azhar Zawawi wrote the paper. All authors have read and approved the final manuscript.

References

1. Olivier-Bourbigou, H.; Magna, L.; Morvan, D. Ionic liquids and catalysis: Recent progress from knowledge to applications. *Appl. Catal. A Gen.* **2010**, *373*, 1–56. [CrossRef]

2. Plechkova, N.V.; Seddon, K.R. Applications of ionic liquids in the chemical industry. *Chem. Soc. Rev.* **2008**, *37*, 123–150. [CrossRef] [PubMed]

3. Siedlecka, E.M.; Fabiańska, A.; Stolte, S.; Nienstedt, A.; Ossowski, T.; Stepnowski, P.; Thöming, J. Electrocatalytic Oxidation of 1-Butyl-3-Methylimidazolium Chloride: Effect of the Electrode Material. *Int. J. Electrochem. Sci.* **2013**, *8*, 5560–5574.

4. Munoz, M.; Domínguez, C.M.; de Pedro, Z.M.; Quintanilla, A.; Casas, J.A.; Rodriguez, J.J. Ionic liquids breakdown by Fenton oxidation. *Catal. Today* **2015**, *240*, 16–21. [CrossRef]

5. Zhou, H.; Shen, Y.; Lv, P.; Wang, J.; Li, P. Degradation pathway and kinetics of 1-alkyl-3-methylimidazolium bromides oxidation in an ultrasonic nanoscale zero-valent iron/hydrogen peroxide system. *J. Hazard. Mater.* **2015**, *284*, 241–252. [CrossRef] [PubMed]

6. Buthiyappan, A.; Abdul Aziz, A.R.; Wan Daud, W.M.A. Recent advances and prospects of catalytic advanced oxidation process in treating textile effluents. *Rev. Chem. Eng.* **2016**, *32*, 1–47. [CrossRef]

7. Ramli, R.M.; Chong, F.K.; Omar, A.A. Visible-Light Photodegradation of Diisopropanolamine Using Bimetallic Cu-Fe/TiO_2 Photocatalyst. *Adv. Mater. Res.* **2013**, *845*, 421–425. [CrossRef]

8. Ramli, R.M.; Kait, C.F.; Omar, A.A. Remediation of DIPA contaminated wastewater using visible light active bimetallic Cu-Fe/TiO_2 Photocatalyst. *Procedia Eng.* **2016**, *148*, 508–515. [CrossRef]

9. Saepurahman; Abdullah, M.A.; Chong, F.K. Preparation and characterization of tungsten-loaded titanium dioxide photocatalyst for enhanced dye degradation. *J. Hazard. Mater.* **2010**, *176*, 451–458. [CrossRef] [PubMed]

10. Ramli, R.M.; Kait, C.F.; Omar, A.A. Photodegradation of aqueous diisopropanolamine using Cu/TiO_2: Effect of calcination temperature and duration. *Appl. Mech. Mater.* **2014**, *625*, 847–850. [CrossRef]

11. Orha, C.; Pode, R.; Manea, F.; Lazau, C.; Bandas, C. Titanium dioxide-modified activated carbon for advanced drinking water treatment. *Process Saf. Environ. Prot.* **2016**, *108*, 26–33. [CrossRef]

12. Sampaio, M.J.; Pastrana-Martinez, L.M.; Silva, A.M.T.; Buijnsters, J.G.; Han, C.; Silva, C.G.; Carabineiro, S.A.C.; Dionysiou, D.D.; Faria, J.L. Nanodiamond-TiO_2 composites for photocatalytic degradation of microcystin-LA in aqueous solutions under simulated solar light. *RSC Adv.* **2015**, *5*, 58363–58370. [CrossRef]

13. Pastrana-Martínez, L.M.; Morales-Torres, S.; Carabineiro, S.A.C.; Buijnsters, J.G.; Faria, J.L.; Figueiredo, J.L.; Silva, A.M.T. Nanodiamond–TiO_2 Composites for Heterogeneous Photocatalysis. *ChemPlusChem* **2013**, *78*, 801–807. [CrossRef]

14. Zhang, D. Enhanced photocatalytic activity for titanium dioxide by co-modification with copper and iron. *Transit. Met. Chem.* **2010**, *35*, 933–938. [CrossRef]

15. Zhou, W.; Zhang, P.; Liu, W. Anatase TiO_2 Nanospindle/ActivatedCarbon (AC) Composite Photocatalysts with Enhanced Activity in Removal of Organic Contaminant. *Int. J. Photoenergy* **2012**. [CrossRef]

16. Ozkal, C.B.; Koruyucu, A.; Meric, S. Heterogeneous photocatalytic degradation, mineralization and detoxification of ampicillin under varying pH and incident photon flux conditions. *Desalin. Water Treat.* **2016**, *57*, 18391–18397. [CrossRef]

17. Zawawi, A.; Ramli, R.M.; Harun, N.Y. Synergistic Effect Of Adsorption-Photodegradation Of Composite TiO_2/AC For Degradation Of 1-Butyl-3-Methylimidazolium Chloride. *Malays. J. Anal. Sci.* **2017**, in press.

18. Di Paola, A.; García-López, E.; Marcì, G.; Martín, C.; Palmisano, L.; Rives, V.; Maria Venezia, A. Surface characterisation of metal ions loaded TiO_2 photocatalysts: structure–activity relationship. *Appl. Catal. B Environ.* **2004**, *48*, 223–233. [CrossRef]

19. Alalm, M.G.; Tawfik, A.; Ookawara, S. Enhancement of photocatalytic activity of TiO_2 by immobilization on activated carbon for degradation of pharmaceuticals. *J. Environ. Chem. Eng.* **2016**, *4*, 1929–1937. [CrossRef]

20. Muhamma, A.S.; Naser, J.T.; Kirm, I.; Jibril, B.Y. Photocatalytic Degradation of Methylene Blue and Phenol Using TiO_2/Activated-Carbon Composite Catalysts. *Asian J. Chem.* **2015**, *1*, 343–348. [CrossRef]

21. Sahoo, S.K.; Agarwal, K.; Singh, A.K.; Polke, B.G.; Raha, K.C. Characterization of γ- and α-Fe_2O_3 nano powders synthesized by emulsion precipitation-calcination route and rheological behaviour of α-Fe_2O_3. *Int. J. Eng. Sci. Technol.* **2010**, *2*, 118–126.

22. Wang, Y.; Muramatsu, A.; Sugimoto, T. FTIR analysis of well-defined α-Fe_2O_3 particles. *Colloids Surf. A Physicochem. Eng. Asp.* **1998**, *134*, 281–297. [CrossRef]

23. Oh, W.C.; Chen, M.L. Formation of TiO_2 composites on activated carbon modified by nitric acid and their photocatalytic activity. *J. Ceram. Process. Res.* **2007**, *8*, 316–323.

24. Wang, X.; Liu, Y.; Hu, Z.; Chen, Y.; Liu, W.; Zhao, G. Degradation of methyl orange by composite photocatalysts nano-TiO_2 immobilized on activated carbons of different porosities. *J. Hazard. Mater.* **2009**, *169*, 1061–1067. [CrossRef] [PubMed]

25. Liu, D.; Wu, Z.; Tian, F.; Ye, B.-C.; Tong, Y. Synthesis of N and La co-doped TiO_2/AC photocatalyst by microwave irradiation for the photocatalytic degradation of naphthalene. *J. Alloys Compd.* **2016**, *676*, 489–498. [CrossRef]

26. Zhang, Z.; Xu, Y.; Ma, X.; Li, F.; Liu, D.; Chen, Z.; Zhang, F.; Dionysiou, D.D. Microwave degradation of methyl orange dye in aqueous solution in the presence of nano-TiO_2-supported activated carbon (supported-TiO_2/AC/MW). *J. Hazard. Mater.* **2012**, *209–210*, 271–277. [CrossRef] [PubMed]

27. Andronic, L.; Enesca, A.; Cazan, C.; Visa, M. TiO_2–active carbon composites for wastewater photocatalysis. *J. Sol–Gel Sci. Technol.* **2014**, *71*, 396–405. [CrossRef]

28. Lemus, J.; Neves, C.M.; Marques, C.F.; Freire, M.G.; Coutinho, J.A.; Palomar, J. Composition and structural effects on the adsorption of ionic liquids onto activated carbon. *Environ. Sci. Process Impacts* **2013**, *15*, 1752–1759. [CrossRef] [PubMed]

29. Lemus, J.; Palomar, J.; Heras, F.; Gilarranz, M.A.; Rodriguez, J.J. Developing criteria for the recovery of ionic liquids from aqueous phase by adsorption with activated carbon. *Sep. Purif. Technol.* **2012**, *97*, 11–19. [CrossRef]

30. Huang, D.; Miyamoto, Y.; Matsumoto, T.; Tojo, T.; Fan, T.; Ding, J.; Guo, Q.; Zhang, D. Preparation and characterization of high-surface-area TiO_2/activated carbon by low-temperature impregnation. *Sep. Purif. Technol.* **2011**, *78*, 9–15. [CrossRef]

31. Xing, B.; Shi, C.; Zhang, C.; Yi, G.; Chen, L.; Guo, H.; Huang, G.; Cao, J. Preparation of TiO_2/Activated Carbon Composites for Photocatalytic Degradation of RhB under UV Light Irradiation. *J. Nanomater.* **2016**. [CrossRef]

32. Qamar, M.; Merzougui, B.; Anjum, D.; Hakeem, A.S.; Yamani, Z.H.; Bahnemann, D. Synthesis and photocatalytic activity of mesoporous nanocrystalline Fe-doped titanium dioxide. *Catal. Today* **2014**, *230*, 158–165. [CrossRef]

33. Nasralla, N.; Yeganeh, M.; Astuti, Y.; Piticharoenphun, S.; Shahtahmasebi, N.; Kompany, A.; Karimipour, M.; Mendis, B.G.; Poolton, N.R.J.; Šiller, L. Structural and spectroscopic study of Fe-doped TiO_2 nanoparticles prepared by sol–gel method. *Sci. Iran.* **2013**, *20*, 1018–1022.

34. Yan, K.; Wu, G.; Jarvis, C.; Wen, J.; Chen, A. Facile synthesis of porous microspheres composed of TiO_2 nanorods with high photocatalytic activity for hydrogen production. *Appl. Catal. B Environ.* **2014**, *148*, 281–287. [CrossRef]

35. Li, Y.; Zhou, X.; Chen, W.; Li, L.; Zen, M.; Qin, S.; Sun, S. Photodecolorization of Rhodamine B on tungsten-doped TiO_2/activated carbon under visible-light irradiation. *J. Hazard. Mater.* **2012**, *227*, 25–33. [CrossRef] [PubMed]

36. Yan, K.; Wu, G. Titanium Dioxide Microsphere-Derived Materials for Solar Fuel Hydrogen Generation. *ACS Sustain. Chem. Eng.* **2015**, *3*, 779–791. [CrossRef]

37. Choi, H.-J.; Kang, M. Hydrogen production from methanol/water decomposition in a liquid photosystem using the anatase structure of Cu loaded TiO_2. *Int. J. Hydrogen Energy* **2007**, *32*, 3841–3848. [CrossRef]

38. Obregón, S.; Lee, S.W.; Rodríguez-González, V. Loading effects of silver nanoparticles on hydrogen photoproduction using a Cu-TiO_2 photocatalyst. *Mater. Lett.* **2016**, *173*, 174–177. [CrossRef]

39. Siedlecka, E.M.; Mrozik, W.; Kaczynski, Z.; Stepnowski, P. Degradation of 1-butyl-3-methylimidazolium chloride ionic liquid in a Fenton-like system. *J. Hazard. Mater.* **2008**, *154*, 893–900. [CrossRef] [PubMed]

40. Tan, Y.N.; Wong, C.L.; Mohamed, A.R. An Overview on the Photocatalytic Activity of Nano-Doped-TiO_2 in the Degradation of Organic Pollutants. *ISRN Mater. Sci.* **2011**, 1–18. [CrossRef]

41. Melcher, J.; Feroz, S.; Bahnemann, D. Comparing photocatalytic activities of commercially available iron-doped and iron-undoped aeroxide TiO_2 P25 powders. *J. Mater. Sci.* **2017**, *52*, 6341–6348. [CrossRef]

42. Senee, K.; Ratchaneekorn, W. Studies on preparation and characterization of Fe/TiO_2 catalyst in photocatalysis applications. *Mater. Res. Express* **2017**, *4*, 076507.

43. Hassena, H. Photocatalytic Degradation of Methylene Blue by Using Al_2O_3/Fe_2O_3 Nano Composite under Visible Light. *Mod. Chem. Appl.* **2016**, *176*. [CrossRef]

44. Alkaim, A.F.; Kandiel, T.A.; Hussein, F.H.; Dillert, R.; Bahnemann, D.W. Enhancing the photocatalytic activity of TiO_2 by pH control: a case study for the degradation of EDTA. *Catal. Sci. Technol.* **2013**, *3*, 3216–3222. [CrossRef]

45. Akpan, U.G.; Hameed, B.H. Parameters affecting the photocatalytic degradation of dyes using TiO_2-based photocatalysts: a review. *J. Hazard. Mater.* **2009**, *170*, 520–529. [CrossRef] [PubMed]

46. Andriantsiferana, C.; Mohamed, E.F.; Delmas, H. Photocatalytic degradation of an azo-dye on TiO_2/activated carbon composite material. *Environ. Technol.* **2013**, *35*, 355–363. [CrossRef] [PubMed]

47. Belver, C.; Bedia, J.; Álvarez-Montero, M.A.; Rodriguez, J.J. Solar photocatalytic purification of water with Ce-doped TiO_2/clay heterostructures. *Catal. Today* **2016**, *266*, 36–45. [CrossRef]